An Online Data-Driven Method for Simultaneous Diagnosis of IGBT and Current Sensor Fault of Three-Phase PWM Inverter in Induction Motor Drives

Bin Gou, *Member, IEEE*, Yan Xu, *Senior Member, IEEE*, Yang Xia, *Student Member, IEEE*, Qingli Deng, *Student Member, IEEE*, and Xinglai Ge, *Member, IEEE*

***Abstract*—This article presents an online data-driven diagnosis method for multiple insulated gate bipolar transistors (IGBTs) open-circuit faults and current sensor faults in the three-phase pulsewidth modulation inverter. The fast Fourier transform (FFT) algorithm is used to extract the fault frequency spectrum features of the three-phase currents. Then, a feature selection method named ReliefF is introduced to select the most critical features by removing redundant and irrelevant features. In addition, as novel fast learning technology, a random vector functional link network is applied to learn the faulty knowledge from the historical dataset. Based on the well-learned model, the fault type and location of the converter can be accurately identified as long as the three-phase current signals are measured. Offline test results verify that the proposed method can identify the IGBT and sensor faults with an accuracy of 98.83% and outperforms the state-of-the-art learning algorithms. Moreover, the real-time hardware-in-the-loop test results show that the proposed method can successfully identify the IGBT faults and current sensor faults within 22 ms. It is robust to the dc-link voltage fluctuations, model parameters, and speed or load variations. The extensibility of the proposed method is also validated based on the test results in terms of other fault modes and drive systems.**

***Index Terms*—Fault diagnosis, insulated gate bipolar transistor (IGBT) open-circuit fault, random vector functional link (RVFL) network, sensor fault, three-phase pulsewidth modulation (PWM) inverter.**

I. Introduction

THE three-phase pulsewidth modulation (PWM) inverter fed induction motor drive system has been widely applied in the industry due to its high performance, high reliability, and simple control structure. Power converter used in the induction motor drive system generally applies to the insulated gate bipolar transistors (IGBTs) or metal–oxide–semiconductor field-effect transistors to adjust the frequency and shape of the output ac voltage of the converter. It was reported that the power semiconductor device was the most fragile component in variable speed drives, especially in high-power applications [1]. Failures in the power semiconductor devices may result in catastrophic failures through fault propagation. Therefore, accurate and fast fault diagnosis is highly desirable for the power converter in high-power applications.

The fault modes in the power semiconductor device are mainly appearing as short-circuit fault and open-circuit fault [2]. Short-circuit fault of the power switch is generally caused by overvoltage, overheating, or incorrect command signals. Once occurred, it may result in an abnormal overcurrent in an extremely short time, e.g., 10 μs, which can cause immediate damage to the power converter [3]. Normally, short-circuit fault is detected and isolated by standard protection circuits in industrial drive applications [4], such as fuse, breaker, or *di/dt* feedback methods [5]. Nevertheless, the open-circuit fault is generally caused by the wire bone failure due to thermomechanical fatigue or loss of command signal [6]. Normally, the open-circuit fault may not make the drive system crash but could degrade the system performance, such as current distortion and electromagnetic torque fluctuation. It may not enable the protection mechanism immediately but may result in some secondary faults, or even shut down the traction drive system [7]. As a result, this article is to diagnose the open-circuit fault in power devices.

Apart from power semiconductor faults, the associated sensor faults, such as voltage and current sensor faults, are also common in the drive system. Sensor fault may result in measurement signal distortion that causes performance degradation or even damages other components due to the closed-loop control strategies of drives. The fault types of the current sensor can be categorized into stuck, offset, and noise fault, according to the measurement result [8].

Over the last decades, the fault diagnosis methods for IGBT or sensor can generally be classified as the model-based method, signal-based method, and knowledge-based method [9], [10]. Observer-based methods [11], [12], parity space methods [13], and parameter estimation techniques [14] are the most representative model-based method. For instance, a sliding mode observer [15] and nonlinear observers [16] are designed to detect the IGBT open-circuit fault in the multilevel converter

Manuscript received January 17, 2020; revised March 13, 2020; accepted May 7, 2020. Date of publication May 13, 2020; date of current version July 31, 2020. This work was supported in part by the National Natural Science Foundation of China under Grants 51907163 and U1934204 and in part by Chengdu Guojia Electrical Engineering Corporation, Ltd., under Grant NEEC-2017-B06. Recommended for publication by Associate Editor B. Mirafzal. *(Corresponding author: Bin Gou.)*

Bin Gou, Qingli Deng, and Xinglai Ge are with the School of Electrical Engineering, Southwest Jiaotong University, Chengdu 610031, China (e-mail: bingo57350@126.com; qinglideng@my.swjtu.edu.cn; xlgee@163.com).

Yan Xu and Yang Xia are with the School of Electrical and Electronic Engineering, Nanyang Technological University, Singapore 639798, Singapore (e-mail: xuyan@ntu.edu.sg; xiay0020@e.ntu.edu.sg).

Color versions of one or more of the figures in this article are available online at https://ieeexplore.ieee.org.

Digital Object Identifier 10.1109/TPEL.2020.2994351

0885-8993 © 2020 IEEE. Personal use is permitted, but republication/redistribution requires IEEE permission.
See https://www.ieee.org/publications/rights/index.html for more information.

Authorized licensed use limited to: JACK YEH. Downloaded on June 20,2024 at 12:42:45 UTC from IEEE Xplore. Restrictions apply.

and induction motor drives, respectively. In addition, a mixed logical dynamic model is set up to detect the IGBT open-circuit fault in a single-phase PWM rectifier [17], [18]. The model-based method is also widely applied to sensor fault diagnosis, such as Luenberger observers [19], sliding mode observers [20], and extended Kalman filters [21]. Hwang *et al.* [22] have discussed various model-based fault detection and reconfiguration methods developed over the last decades. They classify the techniques based on robust residual generation techniques, statistical decision techniques, and reconfiguration control techniques.

IGBT open-circuit faults result in characteristic distortion of current and voltage signals. Thus, the signal-based method is also popular in detecting the power semiconductor device fault and can be generally divided into current-based [23], [24] and voltage-based methods [25], [26]. For the voltage source converter, the current-based method is independent of converter parameters and does not require additional hardware. But it needs a relatively long diagnostic time to guarantee a higher detection accuracy, normally one fundamental period. The terminal voltage of the power semiconductor device expresses fault feature, first, when an open-circuit fault occurs in a voltage source converter. Therefore, the voltage-based method has the fastest diagnostic speed and highest accuracy. However, the voltage-based method normally needs additional voltage sensors, which highly increase the cost and complexity of the system and consequently limit its application. Recently, some new signal-based methods were also proposed to identify the faults in the converter. Abari *et al.* [27] apply the conducted and radiated electromagnetic signatures of the dc bus to detect the open-circuit fault of the clamping diode in the three-level neutral point clamped (NPC) inverter by using an electromagnetic interference filter and external antenna.

Different from the model-based and signal-based methods, the knowledge-based method is independent of the system model, load condition, and signal patterns, but requires a large historical data. Thus, it is also called data-driven method and draws significant attention in fault diagnosis for converters [28], such as fuzzy expert system, support vector machine (SVM), and Bayesian network (BN). For instance, in [29], a fault diagnosis method based on principal component analysis (PCA) and multiclass relevance vector machine (PCA-mRVM) is proposed to diagnose the open-circuit faults in H-bridge multilevel inverter system. In [30], the wavelet packet transform is introduced to extract the fault features, and the long short-term memory algorithm is presented to detect the open-circuit fault and short-short fault in a five-level nested neutral-point-pilot converter. Cai *et al.* [7] proposed a PCA-BN based diagnosis method to detect open-circuit faults in three-phase inverters. In both methods, fast Fourier transform (FFT) is used to preprocess the output voltage signals. In [31], an ensemble intelligent time-adaptive data-driven method based on the extreme learning machine (ELM) is proposed to identify the sensor faults in induction drives, including the current sensor, voltage sensor, and speed sensor.

For the traditional fault diagnosis methods, power semiconductor faults and sensor faults are generally detected independently. However, it is worth noting that the fault features of the power semiconductor and current sensor can be similar in some specific situations. For instance, when the output of the current sensor is stuck at zero value, the fault expression, according to the measurement, is the same as that of open-circuit fault in the converter bridge. Thus, it is highly possible to result in misdiagnosis by using the existing diagnosis methods. Unfortunately, very few works have been reported to identify both the power semiconductor fault and current sensor fault in ac drives, simultaneously.

In [32], a robust observer-based method is proposed for IGBTs and current sensors fault in voltage-source inverters of permanent magnet synchronous motor (PMSM) drives. It is achieved by evaluating the thresholds of residuals obtained by observers. However, it cannot identify the sensor fault types. In [33], a normalized average current method is proposed to detect IGBT open-circuit fault and current sensor fault in permanent magnet synchronous generator (PMSG) drives. Although it can detect the faulty phase, it cannot distinguish the specific faulty switch and the faulty types of sensors.

Many comprehensive survey articles also summarize the fault diagnosis techniques reported over the last decades. In [9] and [10], the advantages and constraints of model-based, signal-based, knowledge-based, and hybrid diagnosis techniques are evaluated. Literature [34] has compared the effectiveness, resistivity, and detection time of the IGBT diagnostic and protection methods for power inverters.

This article also evaluates and compares the cited fault diagnostic methods comprehensively in terms of fault modes, detection variables, tuning effort, effectiveness, detection time, and implementation effort, illustrated in Table I. In summary, for the model-based method, the system identification methods or physical principles are introduced to emulate the practical system and generate system residuals by comparing the measured outputs and model-predicted outputs. It is fast and load-independent since the diagnostic time is only decided by the evaluation threshold value of the system residual. However, it has poor resistivity for parameter variation and noise interference. For the signal-based method, various signal process methods are adopted to extract the fault symptoms. It is independent of the physical model, but always suffers from the long diagnostic time and is significantly sensitive to the system load. Both model- and signal-based methods are only based on the online measurement results to detect the fault location. In contrast, the data-driven method is by learning the mapping-knowledge relationship between the fault characteristics and fault modes from the historical data and online monitored data. It is independent of the system model and load variation. However, the data-driven method is always judged difficult for real-time applications due to its heavy training and computational burden.

To overcome the drawbacks of the traditional fault diagnostic methods, this article proposes an online fault diagnosis method based on the data-driven technology to simultaneously identify multiple IGBT faults and current sensor faults. The inputs of the proposed method are only the three-phase current signal measurements of the inverter, and outputs are fault types and locations. The contributions are summarized as follows.

Authorized licensed use limited to: JACK YEH. Downloaded on June 20,2024 at 12:42:45 UTC from IEEE Xplore. Restrictions apply.

TABLE I
COMPARISON OF IGBT AND SENSOR FAULT DIAGNOSTIC METHODS

Methods	Research Plant	Faulty Modes	Detection Parameter	Tuning Effort	Effectiveness	Detection Time	Implementation Effort
Instant voltage error based method [2]	3-level NPC rectifier	IGBT open-circuit fault	Control states, current and line voltage signals	Medium	Good	80 *u*s to 3 ms	Low
Hardware based method [3]	Cascaded H-Bridge multilevel converter	IGBT open-circuit fault	New current and voltage signals	Low	Good but require additional current and voltage sensors	< one Fundamental Period (FP)	High
di/dt feedback based method [5]	IGBT	Short-circuit protection	Current and voltage signals	Low	Good	2 *u*s	Medium
Model reference adaptive system method [6]	PWM inverter in PMSM drives	IGBT open-circuit fault	PMSM model	Low	Good but sensitive to parameters	< 1 ms	Low
Bayesian network method [7]	PWM inverter in PMSM drives	IGBT open-circuit fault	Line-to-line voltage signals	High	Offline-test is good	No online test	Medium
Support vector machine based method [8]	Temperature sensor	Sensor fault	Sensor signal	High	Offline-test is good	No online test	Medium
State-space observer [11]	Four-phase interleaved buck converter	Phase open-circuit fault	Input and output DC-link voltage and total current	Medium	Good but ambiguous at small currents	0.1 ms	Low
Full-order observers [12]	Voltage source inverter	Current sensor fault	Current signals, command and speed signals	Low	Good but unsatisfied at low speed	≈ 20 ms	Medium
Parity space approach [13]	Voltage source inverter	Current sensor fault	Three-phase currents	Medium	Good	2.52 us	Medium
Sliding mode observer [15]	Modular multilevel converters	Switch open-circuit fault	Current and voltage signals	Low	Good but sensitive to data error	100 ms	Low
Nonlinear observers [16]	Voltage source inverter	IGBT open-circuit fault	Induction motor model	Medium	Sensitive to model parameters	≈ 30 ms	Medium
Mixed logical dynamic model [17] [18]	Single phase PWM rectifier	IGBT open-circuit fault	DC-link voltage, switch signals	Low	Good	3 ms	Low
Luenberger observers [19]	Single phase PWM rectifier	Catenary current sensor and DC voltage sensor	Single phase rectifier model	Medium	Good	0.3 ms	Low
Sliding mode observers [20]	Single phase PWM rectifier	Catenary current sensor and DC voltage sensor	Single phase rectifier model	Medium	Good	2.3 ms	Medium
Extended Kalman filters [21]	PMSM drives	DC-link voltage, currents, and position sensor	PMSM model	Medium	Poor at low speed and sensitive to parameters	Not Available	Medium
Current signal based method [23]	Back-to-back converters	IGBT open-circuit fault	Three-phase currents	Low	Good	> one FP	Low
Load current signal based method [24]	Voltage source inverter	IGBT and current sensor	Three-phase currents	Low	Good	one FP	Low
Voltage similarity-based method [25]	Modular multilevel converters	IGBT open-circuit fault	Submodule capacitor voltage	Low	Good but not suitable for multiple faults	Within one FP	Low
Model-predictive control method [26]	Modular multilevel converters	IGBT open-circuit fault	Arm voltage	Low	Good but not suitable for multiple faults	Several sampling periods	Low
Electromagnetic signal based method [27]	3-level NPC inverter	IGBT open-circuit fault	DC-bus electromagnetic signatures	Medium	Good but needs an EMI filter	Half of FP	Medium
Artificial neural network based method [28]	AC–DC converter	Open-phase fault	DC-bus current	High	Needs DC-bus current	Not Available	High
mRVM method [29]	Cascaded H-Bridge multilevel inverter	IGBT open-circuit fault	Output voltages	High	Good	> 20 ms	High
Long short-term memory based method [30]	Five-level converter	IGBT fault	Output voltages	High	Good	> 24 ms	High
Ensemble extreme learning machine based method [31]	Voltage source inverter	DC-voltage, current, and speed sensors	DC -voltage, currents, and speed signals	High	Good	9.71 ms	High
Robust observer-based method [32]	PMSM drives	IGBTs and current sensors	PMSM model	Medium	Good	≤ 58% of FP	Medium
Current signal based method [33]	PMSG drives	IGBTs and current sensors	Phase current signals	Low	Good but not clear at small currents	≤ 50% of FP	Low

Authorized licensed use limited to: JACK YEH. Downloaded on June 20,2024 at 12:42:45 UTC from IEEE Xplore. Restrictions apply.

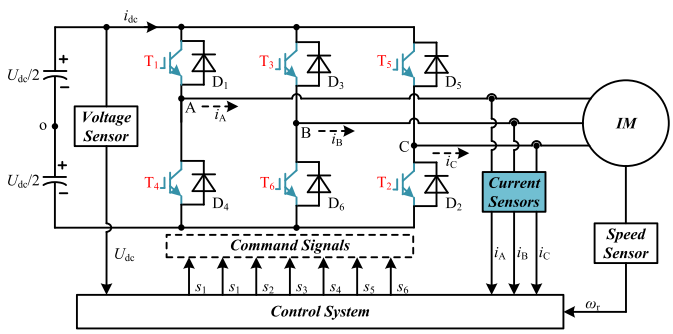

Fig. 1. Structure of a three-phase inverter fed induction motor drive system.

1) Both the IGBT open-circuit faults and sensor faults in an induction motor drive system are investigated. The proposed method can achieve a simultaneous online diagnosis of the fault type and fault location.
2) A feature extraction and selection method based on FFT and ReliefF are respectively proposed to select the most critical fault character frequency as the model inputs. The dimensionality of the feature inputs is also reduced, which highly reduces the training and computational burden.
3) A fast and accurate machine learning technique named random vector functional link (RVFL) network is applied to learn the fault data. The unique structure of the RVFL network has a better balance between diagnostic speed and accuracy.
4) The generalization performance of the proposed data-driven method is validated based on the tests of additional fault modes and different converter topology.

II. Description and Fault Labeling

In the high-speed railway, the ac power drive system consists of a three-phase PWM inverter and an induction motor, as shown in Fig. 1. Each phase of the two-level inverter has two power switches, T_i, and two antiparallel diodes, D_i.

A. IGBT Open-Circuit Fault Analysis

When the open-circuit fault occurs in the upper switch of leg A T_1, the dc-link current i_{dc} could not flow through the power switch T_1, which means there is no positive part of the current i_A. Meanwhile, there are positive bias components in the currents of phases B and C, since the winding connection of the induction motor is star type and has no neutral point. Similarly, there is no negative part current when switch T_4 is in open-circuit fault and no current signal when both T_1 and T_4 are in open-circuit fault.

In practice, very rare a case of more than two IGBTs experiences fault simultaneously. Thus, only single and double IGBTs open-circuit faults are considered in this article. It can be summarized that there is a total of 21 fault modes, including single and double IGBT open-circuit faults.

TABLE II
Labeling of Inverter Faults

Fault modes	Label	Fault modes	Label
No Fault	1	T_3&T_4 Open-circuit Fault	17
T_1 Open-circuit Fault	2	T_3&T_5 Open-circuit Fault	18
T_2 Open-circuit Fault	3	T_3&T_6 Open-circuit Fault	19
T_3 Open-circuit Fault	4	T_4&T_5 Open-circuit Fault	20
T_4 Open-circuit Fault	5	T_4&T_6 Open-circuit Fault	21
T_5 Open-circuit Fault	6	T_5&T_6 Open-circuit Fault	22
T_6 Open-circuit Fault	7	Sensor A Stuck Fault	23
T_1&T_2 Open-circuit Fault	8	Sensor B Stuck Fault	24
T_1&T_3 Open-circuit Fault	9	Sensor C Stuck Fault	25
T_1&T_4 Open-circuit Fault	10	Sensor A Offset Fault	26
T_1&T_5 Open-circuit Fault	11	Sensor B Offset Fault	27
T_1&T_6 Open-circuit Fault	12	Sensor C Offset Fault	28
T_2&T_3 Open-circuit Fault	13	Sensor A Noise Fault	29
T_2&T_4 Open-circuit Fault	14	Sensor B Noise Fault	30
T_2&T_5 Open-circuit Fault	15	Sensor C Noise Fault	31
T_2&T_6 Open-circuit Fault	16		

B. Sensor Fault Definition and Analysis

Generally, there are three current sensors equipped in the inverter to satisfy the safety-critical demand of a high-speed railway drive system. As defined in [31], the fault types of the current sensor can be summarized as a stuck fault, offset fault, and noise fault, according to the measurement result.

In order to analyze the fault effects and phenomena, an offset fault is supposed to introduce into the current sensor of phase A. Since the indirect field-oriented control scheme is applied in the induction motor drive system, there are evident deviations in the feedback currents of exciting current component and torque current component that can be achieved by a coordinate transformation. This dynamic regulation process could result in a difference between the output of the current sensor and that of the inverter. When the offset fault occurs, there are noteworthy dc components in three-phase currents, which could lead to a sharp increase in the motor temperature and fluctuation in electromagnetic torque. Similarly, the stuck fault could lead to a distortion of the current or even make the system shutdown. In addition, noise fault may result in a signal precision reduction, which consequently generates fluctuation in electromagnetic torque.

In summary, there are 21 and 9 operation statuses for IGBT faults and current sensor faults, respectively. To diagnose the fault of the inverter means to identify the operation status. Therefore, fault label is introduced to describe the operation statuses of the inverter.

C. Labeling of Faults

The labels of the inverter for IGBT multiple open-circuit faults and current sensor faults can be defined in Table II. Each label represents the operation status of the inverter. Thus, there are 31 operation statuses of the inverter, including normal situation, single IGBT open-circuit faults, double IGBTs open-circuit faults, and current sensor stuck, offset, and noise faults. Consequently, the proposed fault diagnosis method is to identify the fault label based on well-learned knowledge from the historical data.

Authorized licensed use limited to: JACK YEH. Downloaded on June 20,2024 at 12:42:45 UTC from IEEE Xplore. Restrictions apply.

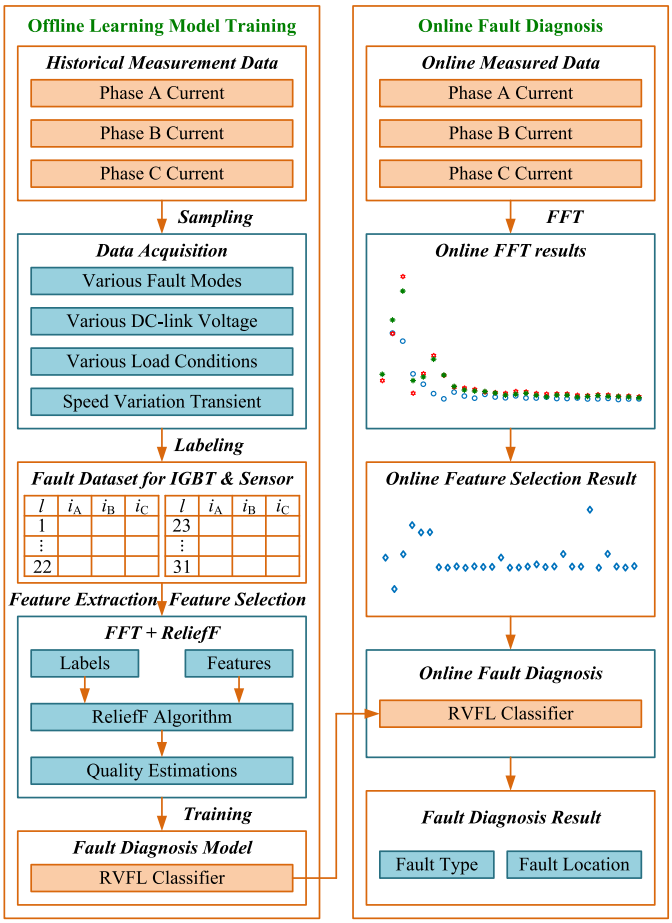

Fig. 2. Proposed fault diagnosis structure based on the RVFL network learning method.

III. Proposed Method

The proposed fault diagnosis structure based on the RVFL network for the three-phase PWM inverter can be illustrated in Fig. 2. The basic idea of the proposed data-driven method is to identify the fault labels by extracting the mapping relationship between the fault characteristics and the corresponding fault labels using the RVFL network. It comprises of the offline training part and the online diagnosis process.

For the offline training part, only three-phase currents of the inverter under various operation conditions are collected to generate the original database. FFT algorithm is used to extract the fault frequency features of the three-phase currents. ReliefF algorithm is applied to weight the most related fault features, which can reduce the feature dimensions and cut down the computational cost. The selected frequency sets are used as the input of the RVFL network for training and testing. A large proportion of instances from the database are randomly selected for model training, while the rest instances are used for model validation. RVFL network is applied as a classification learner to extract the knowledge relationship between the selected frequency components and the fault labels of the inverter. After that, a well-trained learning model, which contains the *a priori* knowledge of IGBT and sensor faults, is achieved.

For the online diagnosis process, the frequency spectrums of the three-phase currents are calculated by the FFT algorithm. The most critical frequency features are selected according to the evaluation results of the ReliefF algorithm in the offline training process. It is worth noting that the ReliefF algorithm only works in the offline training section. Then, the selected frequency features are imported to the well-trained model to calculate the fault label, which indicates the fault type and fault location.

A. Data Acquisition

The database is the foundation to guarantee the high accuracy and reliability of the diagnosis method. There is a total of 31 operation statuses of the inverter, as illustrated in Table II. The operational data under various operating conditions should be collected, such as the time-varying catenary voltage and speed, dc-link ripple voltage, and different operation modes of induction motor (e.g., traction mode and regenerative brake mode).

B. Feature Extraction and Feature Selection

For machine learning, as the dimensionality of the data rises, the computational time grows exponentially. Dimensionality reduction is normally an indispensable step for machine learning to effectively remove the irrelevant and redundant data, increase the learning accuracy and efficiency, and improve result comprehensibility. In this article, FFT is adopted to extract the frequency spectrum features of the three-phase currents of the converter. A feature selection method named ReliefF is introduced to select the most critical fault features by removing the redundant and irrelevant features.

ReliefF [35] is a well-known feature-weighting approach for feature estimation and selection. It is the extension of the original Relief algorithm [36], which was designed for two-class problems without missing values. The original Relief algorithm consists of iteratively updating the weight for each feature by

$$W[F_i] = W[F_i] - \mathrm{diff}(F_i, \mathbf{x}_k, \mathbf{x}_H)/m + \mathrm{diff}(F_i, \mathbf{x}_k, \mathbf{x}_M)/m \tag{1}$$

where F_i denotes a feature, $\mathbf{x}_k$ is the instance sampled in the ith iteration, $i \leq m$, and $\mathbf{x}_H$ and $\mathbf{x}_M$ are the nearest instances from the same and different class with $\mathbf{x}_k$, called nearest hit and nearest miss, respectively. m is the number of sampled instances. Function $\mathrm{diff}(F_i, \mathbf{x}_{k1}, \mathbf{x}_{k2})$ is used for calculating the distance between instances when finding the nearest neighbors can be illustrated as

$$\mathrm{diff}(F_i, \mathbf{x}_{k1}, \mathbf{x}_{k2}) = \frac{|\mathrm{value}(F_i, \mathbf{x}_{k1}) - \mathrm{value}(F_i, \mathbf{x}_{k2})|}{\max(F_i) - \min(F_i)}. \tag{2}$$

For the converter fault diagnosis, it is a multiclassification problem. But the original Relief algorithm can only deal with the two-class problem and is sensitive to noise. Therefore, it is extended to be ReliefF with the following weight updating

Authorized licensed use limited to: JACK YEH. Downloaded on June 20,2024 at 12:42:45 UTC from IEEE Xplore. Restrictions apply.

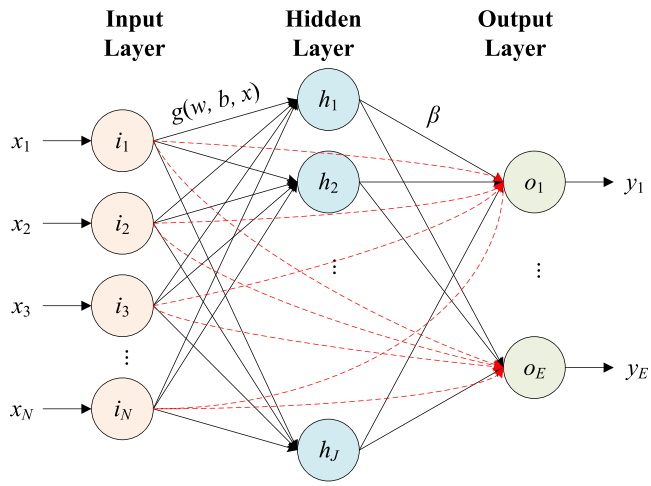

Fig. 3. Structure of the RVFL network.

equation to solve the multiclassification problem [35]:

$$W[F_i]^{i+1} = W[F_i]^i - \sum_{j=1}^{k} \mathrm{diff}(F_i, \mathbf{x}_k, \mathbf{x}_{H,j})/(m \cdot k) + \sum_{C \neq \mathrm{class}(\mathbf{x}_k)}^{k} \left[\frac{P(C)}{1 - P(\mathrm{class}(\mathbf{x}_k))} \cdot \sum_{j=1}^{k} \mathrm{diff}(F_i, \mathbf{x}_k, \mathbf{x}_{M,j}(C))/(m \cdot k) \right] \quad (3)$$

where C is a class label, $P(\cdot)$ is the prior probability of a class, and k is a user-defined parameter.

Instead of n nearest hits and misses, ReliefF searches for n nearest instances from each class. The contributions of different classes are weighted with their prior probabilities. Thus, ReliefF is used for evaluating the feature quality in multiclass problems and able to deal with incomplete and noisy data.

In summary, the basic idea is to measure the relevance of features in the neighborhoods around target samples. For each target sample, ReliefF finds the nearest sample in the feature space of the same category and the other category and uses the difference between those measured distances as the weight of the target feature. For each candidate feature, the importance weight is in the interval $[-1, 1]$, where a positive weight value means the feature can distinguish the instances, while a negative weight value indicates the feature is irrelevant or redundant. Consequently, the features with high positive weights are selected as critical features.

C. RVFL Neural Network

The RVFL was first proposed in 1994, which is a randomized learning algorithm and combines functional link together [37]. It is a single hidden layer feedforward neural network with direct connections from the input layer to the output layer, i.e., as illustrated by the red arrows in Fig. 3. It maps the initial input data $\mathbf{X} = [x_1, x_2, \ldots, x_{\mathrm{N}}]$ to the hidden layer via g $(\omega Tj\mathbf{X} + b_j)$, where g$(\cdot)$ is a nonlinear activation function, ω_{j} is the weights of the jth hidden node, and $\mathrm{b_j}$ is the bias. Combining the direct and hidden nodes connections, the RVFL network can be represented as

$$f(\mathbf{X}) = \sum_{j=1}^{J} \beta_j g(\omega_j^T \mathbf{X} + b_j) + \sum_{j=J+1}^{J+N} \beta_j x_j \quad (4)$$

where J is the total number of hidden nodes, N is the total number of input nodes, and β_{j} is the jth weight terms.

The training of an RVFL network is to minimize the squared output error (ε^2) by finding the optimal hidden layer weights and output layer weights

$$\min \varepsilon^2 = \frac{1}{2P} \sum_{p=1}^{P} \left(t^{(p)} - B^t d^{(p)}\right)^2 \quad (5)$$

where $\mathrm{B^t}$ consists of the (J +N) weight values, P is the total number of training samples, t is the target vector, d is a vector including output nodes, and (p) is the sample index. The weights between the input and hidden layer neurons are randomly sampled from a uniform distribution in $[-1, 1]$. The weights between the hidden and output layer neurons are optimized by the least-squares method. Thanks to the randomized mechanism of the RVFL network, the learning speed could be thousands of times faster than other traditional learning algorithms, which can strongly reduce the training burden.

For the converter fault diagnosis in this article, it is a multiclassification problem. The index of the multioutput nodes of RVFL with the highest value is selected as the predicted label. For example, given a training sample $\mathbf{X}$, the multioutput nodes of RVFL can be represented by $f(\mathbf{X}) = [f_1(x), \ldots, f_E(x)]$, where E is the number of output nodes and is 31 in this article. Then the universal decision function of the RVFL classifier with multioutputs is

$$\mathrm{label}(x) = \arg\max_i f_i(x), \ i \in [1, \ldots, E]. \quad (6)$$

IV. Simulation and Experimental Validations

In this article, the practical electric power drive system of the high-speed train named China railway high-speed (CRH3) is introduced to verify the effectiveness of the proposed online data-driven fault diagnosis method. The drive system consists of a catenary, a traction transformer, two parallel single-phase PWM rectifiers, a three-phase PWM inverter, and four induction motors, as shown in Fig. 4.

A. Real-Time Hardware-in-the-Loop Validation Platform

A real-time hardware-in-the-loop platform is set up to validate the proposed diagnosis method, shown in Fig. 5. The platform has a Raspberry Pi 3 microcontroller to generate the switch PWM signals of IGBTs and implement the proposed diagnostic algorithm, an Opal-RT OP4510, as a hardware-in-the-loop simulator, and a computer as a control interface.

The structure of the platform is illustrated in Fig. 6. The hardware circuits of the traction drive system (as shown in Fig. 4) are simulated in the Opal-RT simulator. The IGBT open-circuit fault

Authorized licensed use limited to: JACK YEH. Downloaded on June 20,2024 at 12:42:45 UTC from IEEE Xplore. Restrictions apply.

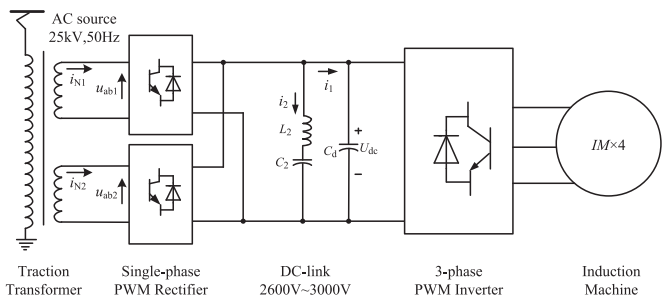

Fig. 4. Strucutre of the ac–dc–ac railway traction system.

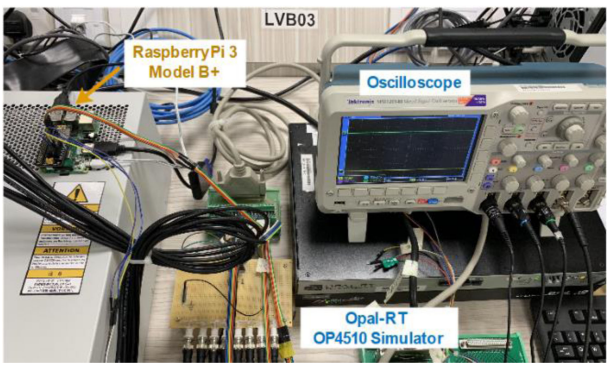

Fig. 5. Hardware-in-the-loop platform.

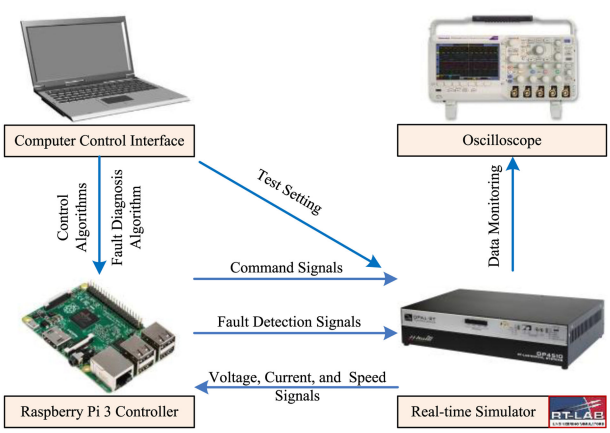

Fig. 6. Structure of the hardware-in-the-loop platform.

is simulated by disabling the corresponding command signal, and sensor faults are emulated according to the definition in [31]. Both the model and control parameters of simulation and experiment are the same and comply with the high-speed train named CRH3, summarized in [31]. For the CRH3, a hybrid modulation strategy is used in the three-phase PWM inverter, including the asynchronous modulation and synchronous modulation, since the conventional asynchronous modulation will generate too many harmonics in the medium-voltage and high-speed drive system due to the limited switching frequency. In addition, the indirect field-oriented control scheme is applied in the inverter and motor control unit.

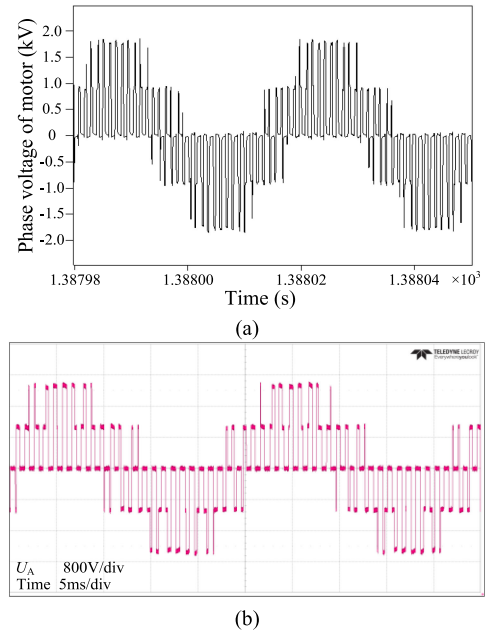

Fig. 7. Phase voltage signal (a) sampling from the real drive of the high-speed train CRH3 and (b) sampling from the hardware-in-the-loop platform.

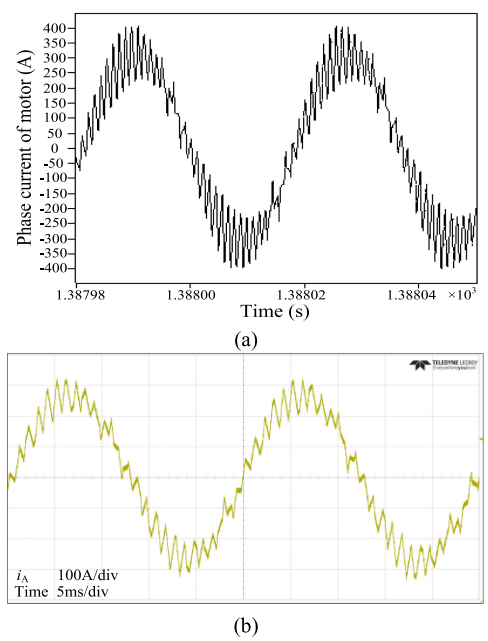

Fig. 8. Phase current signal (a) sampling from the real drive of the high-speed train CRH3 and (b) sampling from the hardware-in-the-loop platform.

B. Model Validation Results

The simulation model working in the simulator is verified with the real data of CRH3. The model validation structure is same as Fig. 6. The controller is a real traction control unit from CRH3. Figs. 7 and 8 show the comparison results between the real operational data from the high-speed train CRH3 and the simulated data from the hardware-in-the-loop platform.

Authorized licensed use limited to: JACK YEH. Downloaded on June 20,2024 at 12:42:45 UTC from IEEE Xplore. Restrictions apply.

TABLE III
DATA ACQUISITION UNDER DIFFERENT FAULT STATUSES AND OPERATION CONDITIONS

	Catenary harmonic voltage	Reference voltage of DC-link	Reference speed	Traction mode	Regenerative braking mode
Simulation data	50 (100 V : 5 kV/100 V)	50 (2.9 : 3.1 kV/4 V)	50 (2 : 100/2 rad/s)	4650 sets	4650 sets
Hardware-in-the-loop data	5 (1 kV : 5 kV/1000 V)	5 (2.9 : 3.1 kV/40 V)	5 (20: 100/20 rad/s)	465 sets	465 sets

It is shown that the platform can accurately emulate the hardware circuit of the real traction drive system in CRH3. Consequently, the hardware-in-the-loop platform is effective to test the effectiveness of the proposed fault diagnosis method.

C. Data Acquisition Results

As illustrated in Table II, there are a total of 31 operation statuses. The data are collected by combining the hardware-in-the-loop model and simulation model of the electric traction drive system of CRH3. The simulation model is based on MATLAB/Simulink software.

To validate the reliability and accuracy of the proposed diagnosis method online, the operational data under various operating conditions are collected, such as the time-varying catenary voltage and speed, dc-link ripple voltage, and different operation modes of induction motor (traction mode and regenerative brake mode). In order to collect more practical operational data, the catenary voltage measured from the real CRH3 train is used as the ac source data of the drive system model. The data acquisition setting are summarized as the following.

1) Harmonic components of catenary voltage (3rd, 5th, and 7th) vary from 100 V to 5 kV with an interval of 100 V.
2) The reference voltage of dc link varies from 2.9 to 3.1 kV with an interval of 4 V.
3) The reference speed of the induction motor varies from 2 to 100 rad/s with an interval of 2 rad/s.

Except for the simulation data, the real-time hardware-in-the-loop sampling data are also collected to enrich the database. The parameters and operating conditions are the same, but the variables interval of the real-time test is ten times larger than the simulation data to save the data acquisition time. The data acquisition process are summarized in Table III. Considering 31 fault statuses of converter, traction, and regenerative brake mode, a total of 10 230 instances of data for the RVFL network can be sampled.

In this article, tenfold cross-validation technology is introduced to verify the performance of the proposed method. In tenfold cross-validation, the samples obtained in Section IV-A are randomly divided into ten equal-sized subsamples. Among the ten subsamples, a single subsample is retained as the validation data, and the remaining night subsamples are used as the training data. The cross-validation process is then repeated ten times, thereby, the classification result is the average value of the ten validations. Therefore, 10% of the acquired dataset is randomly selected as testing data and the remnant samples serve as training data. As a result, there are a total of 1023 testing and 9207 training samples for RVFL to detect the converter faults.

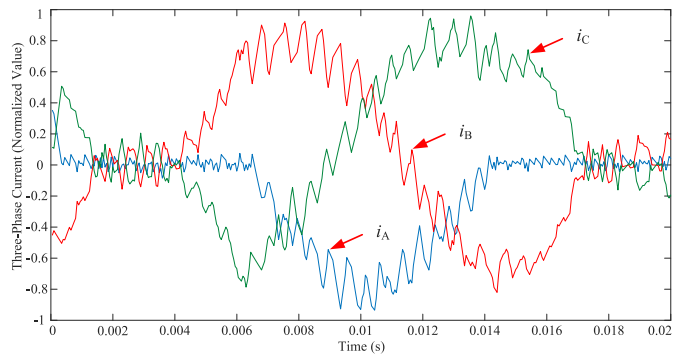

Fig. 9. Three-phase current waveform when T_1 is in open-circuit fault.

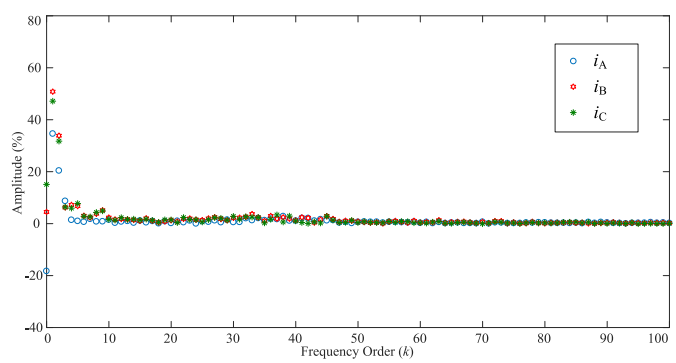

Fig. 10. Corresponding frequency spectrum based on FFT analysis.

D. Feature Extraction and Feature Selection Results

After data acquisition, FFT is adopted to extract the frequency components of the three-phase currents of the inverter. ReliefF is used to weight the relevance of features with the target sample, e.g., the label of the inverter. Assuming that switch T_1 occurs open-circuit fault, the three-phase currents are shown in Fig. 9. The corresponding frequency spectrum based on FFT analysis is illustrated in Fig. 10. There is no positive part of i_A since the dc-link current cannot flow through T_1. As a result, there is a big dc component in the frequency spectrum analysis result of phase A, 19%, as shown in Fig. 10. Fig. 11 illustrates the weight of each frequency component of the three-phase currents. The dc component, fundamental frequency, and the lower order frequency components are the critical features with a bigger weight.

E. Parameters Tuning Results

There are just several parameters of the proposed method needed to be tuned, e.g., the time window for FFT analysis, the

Authorized licensed use limited to: JACK YEH. Downloaded on June 20,2024 at 12:42:45 UTC from IEEE Xplore. Restrictions apply.

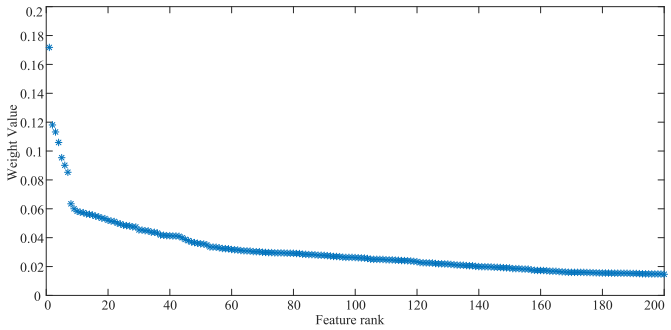

Fig. 11. Weight evaluate value of each frequency order.

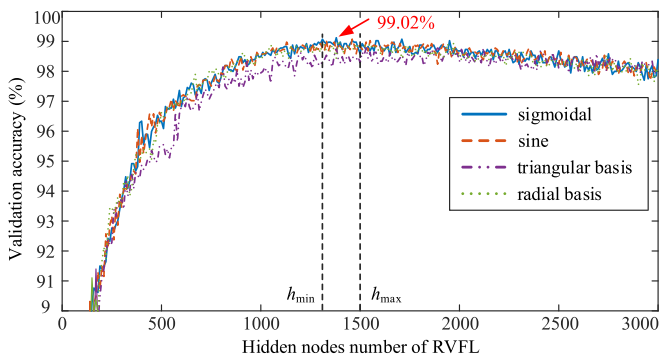

Fig. 12. Single RVFL network hidden nodes versus validation accuracy (%).

number of critical features according to the ReliefF analysis, and the parameters of the RVFL network. Generally, the fundamental period is selected as the time-window for FFT analysis, but it costs a long time for diagnosis in low-speed conditions. To balance the diagnosis time of the whole speed domain, the time-window is selected as 20 ms in this article.

Predictably, a different number of critical features will result in different diagnostic performance. Features that are more critical generally generate higher classification accuracy. However, the more critical features inputs, the larger training time, and computational burden costs. Thus, in this article, the top 30 weights of frequency components are selected as the critical features when balancing the tradeoff between the training accuracy and computing cost. The dimensionality of the input data is reduced highly. Consequently, classification accuracy and computational efficiency are strongly improved.

For the parameters of the RVFL network, one of its advantages is that few user-defined parameters need to be well-tuned offline, namely hidden node number and activation function. The optimal hidden node is selected according to the highest validation accuracy range $[h_{\min}, h_{\max}]$ in this article. Four popular initial activation functions are considered in this article. The highest accuracy by the activation function is selected as the best setting parameters of the RVFL network. The validation result is illustrated in Fig. 12. There is similar validation accuracy for "sigmoidal", "sine", and "radial basis." The highest validation accuracy range is [1300, 1500], where the RVFL network achieves the highest accuracy 99.02%. The activation function is selected as "sigmoidal" since it is very suitable for the classification problem.

F. Offline Validation and Comparison Analysis

To further validate the effectiveness and superiority of the proposed fault diagnosis method, several state-of-the-art data-driven methods used for fault diagnosis are applied to make a fair comparison, as illustrated in Table IV. The tenfold cross-validation method is introduced to compare the performance of the diagnosis methods. The proposed method has the highest training and testing accuracy 99.92% and 98.83%, respectively. In the testing process, only 12 out of 1023 samples are misclassified. Due to the randomized selected input weight, the learning speed of the RVFL network is also very fast. As another random learning algorithm, ELM also has a very fast learning speed. The main difference between ELM and the RVFL network is that the ELM does not have the direct input-output connections, which enhance the stability of the RVFL network. In [31], the ensemble learning structure is proposed to improve the diagnostic accuracy by integrating the outputs of the single ELM classifiers. In this article, the three-phase current trajectories are directly delivered as the inputs of the ELM, which increases the training burden.

For single hidden layer algorithms, the testing time is just decided by the matrix operations of the input features and the trained model. For instance, the classification result of the RVFL learner can be obtained after completing the calculation of (4), which is fast enough for practical online implementation. As a result, the testing time of the compared algorithms is similar. Among them, *k*-nearest neighbor (*k*NN) and decision tree (DT) have the fast training and testing speed, respectively, but relatively lower classification accuracy. The random forest (RF) algorithm has the longest testing time due to the intrinsic ensemble structure. Therefore, RF is hard to be used in the fault diagnosis application of power electronics, although it provides a high classification accuracy at 98.73%.

G. Real-Time Hardware-in-the-Loop Verification

In order to further validate the applicability of the proposed diagnosis method in practical application, some real-time hardware-in-the-loop tests are implemented. The measurement result when the system has no fault is shown in Fig. 13, where CH1 is the fault diagnosis signal, CH2 is the dc-link voltage signal, CH3 is the speed of the motor, and CH4 is the current signal of phase A.

As shown in Fig. 13, the dc-link voltage increases from 2700 V at t_1 and reaches 3600 V to meet the requirement of the constant power control of the drive system. The induction motor starts to brake at t_2 and works as a regenerative braking mode after t_3. The speed of the train increases to 220 km/h until t_3. During the whole operation process, there is no misdiagnosis, even though both the dc-link voltage and train speed vary all the time and the operation mode of the induction motor is changed.

The hardware-in-the-loop test result when switch T_1 occurs open-circuit fault is shown in Fig. 14. The open-circuit fault is introduced at t_0, resulting in a large distortion in the current of phase A. There is no positive component since the dc-link

Authorized licensed use limited to: JACK YEH. Downloaded on June 20,2024 at 12:42:45 UTC from IEEE Xplore. Restrictions apply.

TABLE IV
TENFOLD CROSS VALIDATION WITH OTHER METHODS

Diagnosis method	Training time	Training accuracy	Testing time	Testing accuracy
The proposed method	5.35 s	**99.92 %**	0.58 s	**98.83 %**
FFT+PCA+BN [7]	8.73 s	98.32 %	0.49 s	96.68 %
Time-domain feature extraction + SVM [8]	23.37 s	98.36 %	1.31 s	96.77 %
PCA+mRVM [29]	79.42 s	98.89 %	0.65 s	97.26 %
Ensemble ELM [31]	4 160.15 s	99.00 %	0.78 s	97.36 %
Ensemble RVFL	4 544.32 s	99.29 %	0.79 s	97.75 %
FFT+ReliefF+ELM	3.26 s	99.31 %	0.15 s	97.36 %
FFT+ReliefF+SVM	17.15 s	98.89 %	1.73 s	97.17 %
FFT+ReliefF+kNN	**0.03 s**	98.11 %	0.53 s	96.28 %
FFT+ReliefF+DT	2.57 s	98.32 %	**0.02 s**	94.43 %
FFT+ReliefF+RF	1 532.20 s	99.90 %	35.16 s	98.73 %

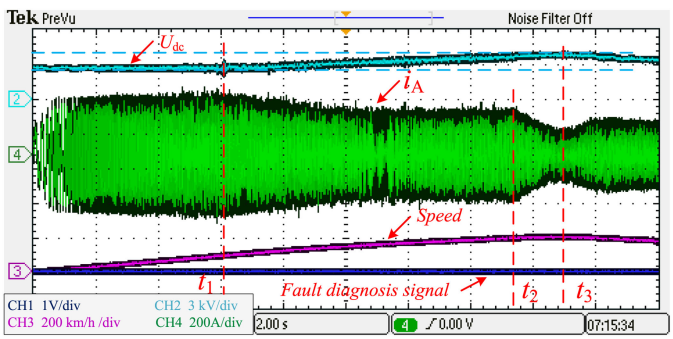

Fig. 13. Hardware-in-the-loop test result in the normal condition (i_A/A, U_{dc}/V, and speed/km/h).

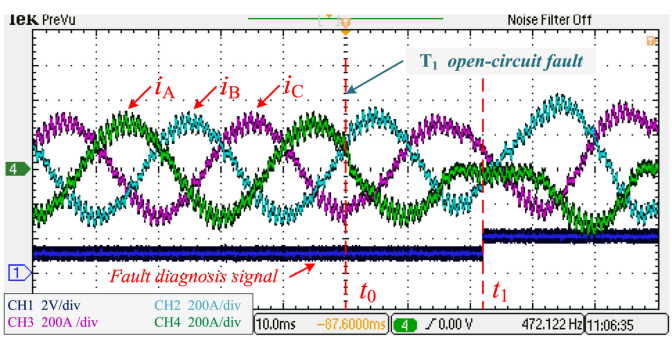

Fig. 14. Hardware-in-the-loop test results when T_1 is in open-circuit fault.

current cannot flow through the T_1. The fault diagnosis signal (CH1) is changed to two from one at t_1, which indicates T_1 is in open-circuit fault, according to Table II. Fig. 15 shows the hardware-in-the-loop test result when both the switch T_1 and T_3 are in open-circuit fault, simultaneously. The three-phase PWM inverter is in synchronous modulation condition. Since both the upper switches of phase A and phase B are open-circuited, the dc-link current can only flow into phase C and flow out from phases A and B. Therefore, there is no positive current component in phase A and phase B and no negative current component in phase C. The fault diagnosis signal changes to nine at t_1, which indicates that the faulty switches are accurately detected according to Table II.

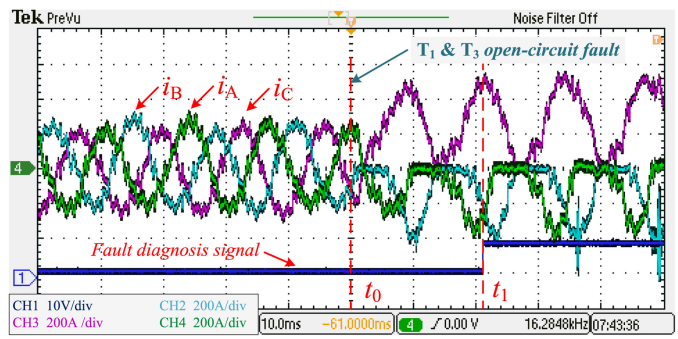

Fig. 15. Hardware-in-the-loop test results when both T_1 and T_3 are in open-circuit fault simultaneously.

To verify the robust performance of the proposed data-driven method, the open-circuit fault is introduced when the induction motor is working in regenerative braking mode, as shown in Fig. 16(a). Fig. 16(b) shows the detailed diagnosis process, where the faulty switches T_1 and T_6 are identified at t_1. It is worth noting that the load of the induction motor is related to the speed of the train. Thus, the proposed method is also robust to the speed and load variation of the motor.

Fig. 17 illustrates the diagnosis result when the current sensor of phase A is in the stuck fault. The diagnosis result is accurately carried out at t_1 before the big distortion of the other two-phase currents. Moreover, the diagnosis result of the offset fault is presented in Fig. 18. DC component of 200 A is added to the output of the current sensor of phase A at t_0. As shown in Fig. 18, there are visible dc offset components in the three-phase currents, although the amplitude of the dc offset components is much lower than that of the injection dc component due to the adjusting ability of the closed-loop control system. The offset fault in the current sensor may not result in a large distortion of current or system shutdown, but it will lead toa sharp increase in the motor temperature and fluctuation electromagnetic torque. The offset fault is also accurately identified at t_1. Fig. 19 shows the noise fault detection result under the regenerative braking mode. A zero-mean white noise Gaussian sequence is introduced in the current sensor of phase A at t_0. The diagnosis result is accurately delivered at t_1.

Authorized licensed use limited to: JACK YEH. Downloaded on June 20,2024 at 12:42:45 UTC from IEEE Xplore. Restrictions apply.

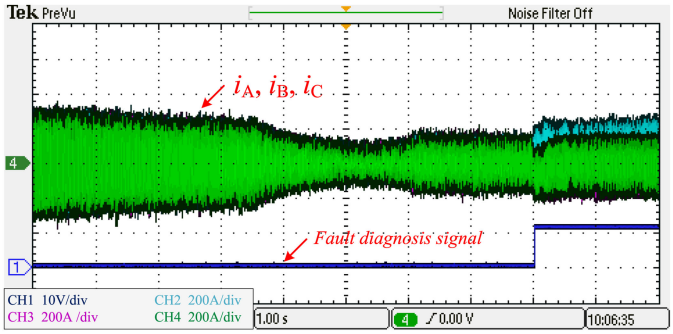

(a)

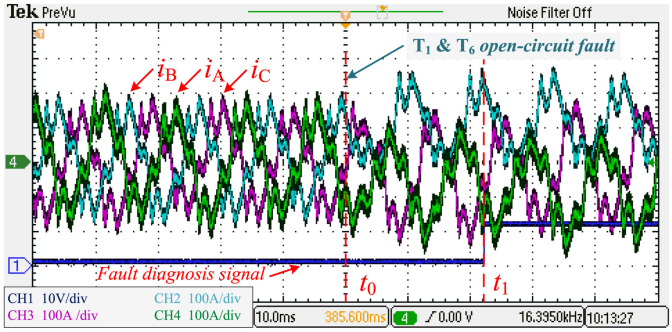

(b)

Fig. 16. Hardware-in-the-loop test results when both T_1 and T_6 are in open-circuit fault, simultaneously, and under regenerative braking mode.

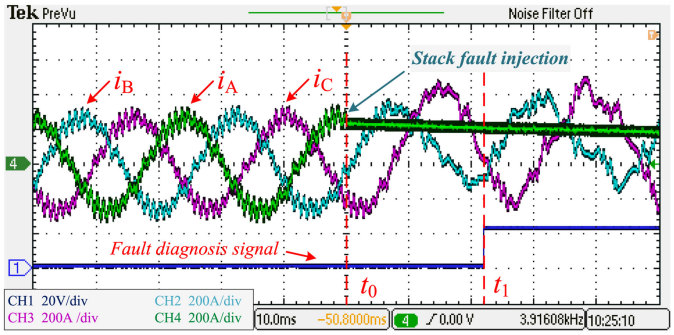

Fig. 17. Hardware-in-the-loop test results when the current sensor of phase A is in stuck fault.

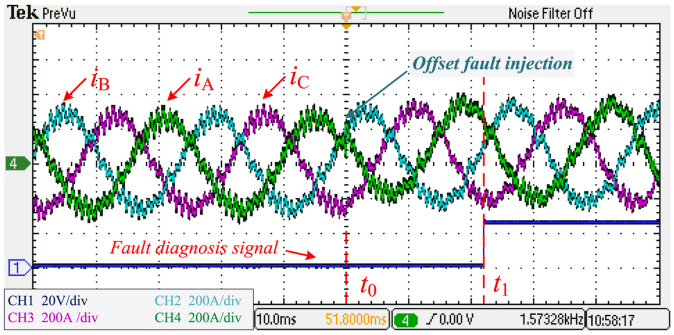

Fig. 18. Hardware-in-the-loop test results when the current sensor of phase A is in offset fault.

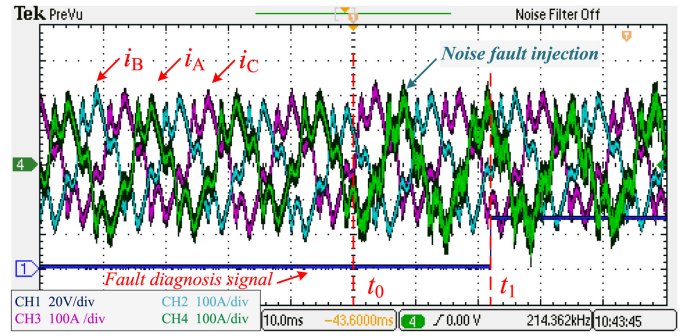

Fig. 19. Hardware-in-the-loop test results when the current sensor of phase A has noise fault and under regenerative braking mode.

TABLE V
COMPLEMENTARY LABELING OF INVERTER FAULTS

Fault modes	Label
DC-link Voltage Sensor Stuck Fault	32
DC-link Voltage Sensor Offset Fault	33
DC-link Voltage Sensor Noise Fault	34
Speed Sensor Stuck Fault	35
Speed Sensor Offset Fault	36
Speed Sensor Noise Fault	37

H. Generalization Performance Verification

It is stated that the data-driven based method has the superiority of generalization. The data-driven based diagnosis method can be easily applied to other fault modes or drive systems. In this article, dc-link voltage sensor faults, speed sensor faults, and three-phase three-level NPC inverter faults are introduced to verify the generalization performance of the proposed method.

1) Verification of Additional Sensor Faults: It is known that in the inverter and induction motor control system of CRH3, there are a dc-link voltage sensor, three-phase current sensors, and a speed sensor used in the control loop. The complementary fault labels are defined in Table V. In order to identify the fault modes of the voltage sensor and speed sensor, the voltage and speed signals are also used as the input of the proposed method. The most correlative fault frequency components of the voltage and speed signals are selected by using FFT and ReliefF algorithm. The top ten weights of the frequency components of the voltage or speed signals are selected as the critical features, respectively.

Fig. 20 shows the diagnosis result when the stuck fault is in the dc-link voltage sensor. The main critical frequency components of the voltage sensor become zero. The stuck fault is accurately identified. Fig. 21 shows the diagnosis result when the noise fault is in the speed sensor. The amplitudes of the fault frequency components increased. It is shown that the proposed method can also accurately identify the senor fault modes in time.

2) Verification of Three-Phase Three-Level NPC Inverter Faults: The verification of the proposed method for diode clamped three-level NPC inverters is implemented. Practically, the traction inverter used in CRH2 is a three-phase three-level

Authorized licensed use limited to: JACK YEH. Downloaded on June 20,2024 at 12:42:45 UTC from IEEE Xplore. Restrictions apply.

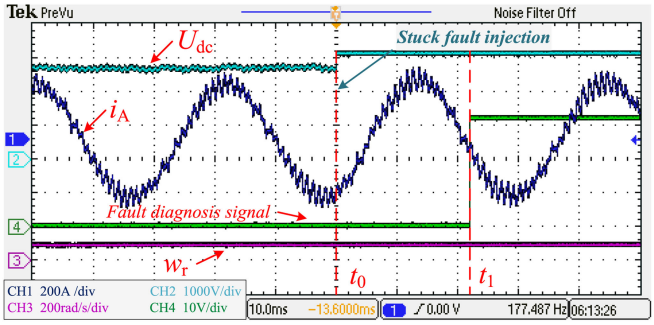

Fig. 20. Hardware-in-the-loop test results when the dc-link voltage sensor is in stuck fault.

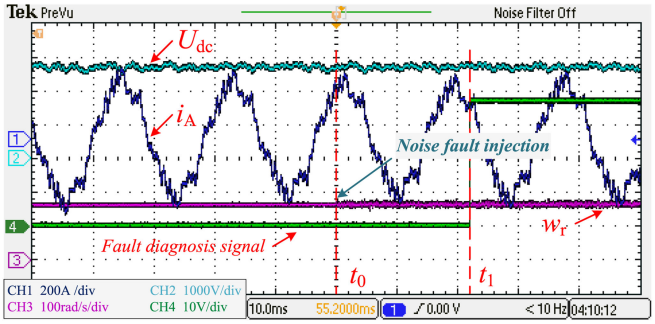

Fig. 21. Hardware-in-the-loop test results when the speed sensor is with a noise fault.

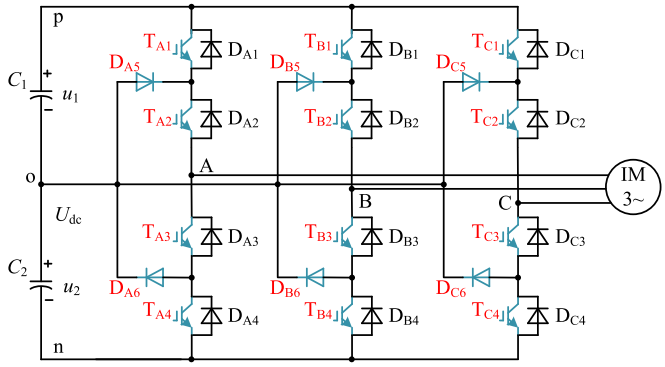

Fig. 22. Structure of three-phase three-level NPC inverter fed induction motor drive circuit.

TABLE VI
LABELING OF THREE-LEVEL NPC INVERTER FAULTS

Fault modes	Label	Fault modes	Label
No Fault	1	T_{C2} Open-circuit Fault	11
T_{A1} Open-circuit Fault	2	T_{C3} Open-circuit Fault	12
T_{A2} Open-circuit Fault	3	T_{C4} Open-circuit Fault	13
T_{A3} Open-circuit Fault	4	D_{A5} Open-circuit Fault	14
T_{A4} Open-circuit Fault	5	D_{A6} Open-circuit Fault	15
T_{B1} Open-circuit Fault	6	D_{B5} Open-circuit Fault	16
T_{B2} Open-circuit Fault	7	D_{B6} Open-circuit Fault	17
T_{B3} Open-circuit Fault	8	D_{C5} Open-circuit Fault	18
T_{B4} Open-circuit Fault	9	D_{C6} Open-circuit Fault	19
T_{C1} Open-circuit Fault	10		

TABLE VII
PARAMETERS OF CONVERTER AND INDUCTION MOTOR

Parameter	Symbol	Value
DC-link voltage	U_{dc}	3000V
DC-link capacitor	C_1=C_2	3.3mF
Highest inverter switching frequency	f_1	1kHz
Stator resistance	R_s	0.144Ω
Stator leakage inductance	L_{ls}	1.417mH
Rotor resistance	R_r	0.816Ω
Rotor leakage inductance	L_{lr}	1.294mH
Mutual inductance	L_m	32.848mH
Rated voltage	U_{rate}	3000V
Rated speed	n_{rate}	4100(r/min)
Rated frequency	f_{srate}	140Hz
Rated output power	P_{rate}	300kW
Number of the pole pairs	np	2

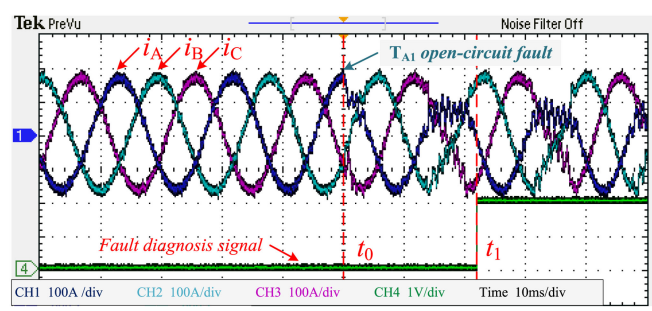

Fig. 23. Hardware-in-the-loop test result when T_{A_1} is in open-circuit fault.

topology. The structure of the three-phase three-level NPC inverter fed induction motor drives is shown in Fig. 22. The open-circuit fault in IGBT and clamp diode is considered, summarized in Table VI. The parameters of the inverter and induction motor are listed in Table VII.

When the IGBT of T_{A_1} occurs open-circuit fault, the clamp diode D_{A_5} is forced to turn ON. But the effective voltage amplitude is decreased. Therefore, the current of the faulty phase is distorted and suppressed. The hardware-in-the-loop test result is shown in Fig. 23. In case of an open-circuit fault occurring in the inner switch T_{A_2}, the dc-link current cannot flow through T_{A_2}. Thus, there is no positive component in the faulty phase, as shown in Fig. 24. When the clamp diode of D_{A_5} occurs open-circuit fault, the antiparallel diodes D_{A_3} and D_{A_4} are forced to turn ON. The load voltage is negative in this case. The fault effects of D_{A_5} and D_{A_6} are similar but the phase angles of the faulty current are different. The hardware-in-the-loop tests when D_{A_5} and D_{A_6} are in open-circuit fault are shown in Figs. 25 and 26, respectively.

In summary, the proposed method can accurately distinguish the IGBT faults and sensor faults and identify the fault type in 22 ms. It is robust to the operation mode of the induction motor and the variation of the dc-link voltage and train speed. The test results of the dc-link voltage sensor, speed sensor, and three-phase three-level NPC inverter verified the versatility and extensibility of the proposed diagnosis method.

Authorized licensed use limited to: JACK YEH. Downloaded on June 20,2024 at 12:42:45 UTC from IEEE Xplore. Restrictions apply.

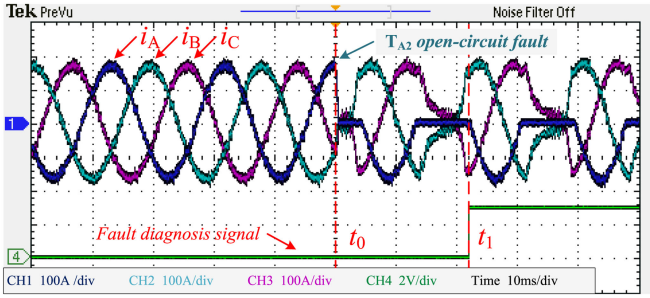

Fig. 24. Hardware-in-the-loop test result when T_{A_2} is in open-circuit fault.

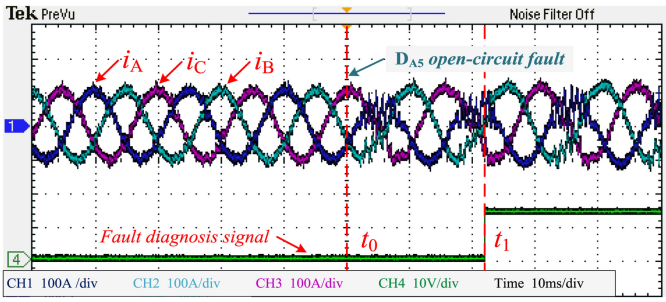

Fig. 25. Hardware-in-the-loop test result when D_{A_5} is in open-circuit fault.

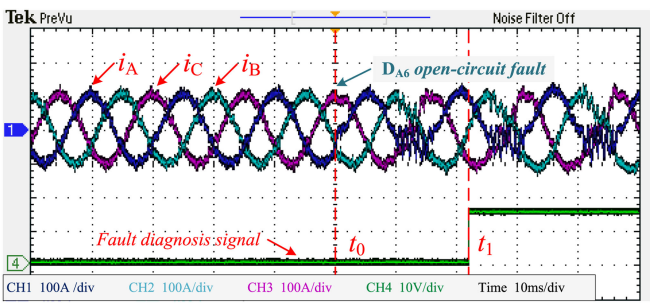

Fig. 26. Hardware-in-the-loop test result when D_{A_6} is in open-circuit fault.

V. Conclusion

This article proposes an RVFL network-based data-driven method for online fault diagnosis of IGBT and the current sensor of inverter in power drive systems.

Considering various fault modes, including multiple IGBT open-circuit fault and current sensors stuck fault, offset fault, and noise fault, the offline tests show that the proposed method well balances the diagnostic speed and accuracy. It can identify the IGBT and sensor faults with an accuracy of 98.83%, which outperforms state-of-the-art learning algorithms. The real-time hardware-in-the-loop test results show that the proposed method can accurately detect the fault mode in 22 ms. The effectiveness and robustness of the proposed method have been validated by the hardware-in-the-loop tests at different load profiles. The results show that the proposed method is also independent of system parameters, which is quite suitable for a nonlinear system, such as the power drive system since the model of induction motor is a high order and nonlinear system with time-varying parameters.

The proposed method is of high expansibility and flexibility. It can detect 30 fault modes of the inverter with high accuracy in this article. In addition, the dc-link sensor fault, speed sensor fault, and three-phase three-level NPC converter faults can also be identified effectively by applying the proposed method structure, as long as the fault data are integrated. A consolidated diagnosis method for the whole system is significant for improving the reliability of the power drive system.

References

[1] S. Yang, A. Bryant, P. Mawby, D. Xiang, L. Ran, and P. Tavner, "An industry-based survey of reliability in power electronic converters," *IEEE Trans. Ind. Appl.*, vol. 47, no. 3, pp. 1441–1451, May/Jun. 2011.

[2] L. M. A. Caseiro and A. M. S. Mendes, "Real-time IGBT open-circuit fault diagnosis in three-level neutral-point-clamped voltage-source rectifiers based on instant voltage error," *IEEE Trans. Ind. Electron.*, vol. 62, no. 3, pp. 1669–1678, Mar. 2015.

[3] J. Lamb and B. Mirafzal, "Open-circuit IGBT fault detection and location isolation for cascaded multilevel converters," *IEEE Trans. Ind. Electron.*, vol. 64, no. 6, pp. 4846–4856, Jun. 2017.

[4] U. Choi, F. Blaabjerg, and K.-B. Lee, "Study and handling methods of power IGBT module failures in power electronic converter systems," *IEEE Trans. Power Electron.*, vol. 30, no. 5, pp. 2517–2533, May 2015.

[5] Z. Wang, X. Shi, L. M. Tolbert, F. Wang, and B. J. Blalock, "A *di/dt* feedback-based active gate driver for smart switching and fast overcurrent protection of IGBT modules," *IEEE Trans. Power Electron.*, vol. 29, no. 7, pp. 3720–3732, Jul. 2014.

[6] S.-M. Jung, J.-S. Park, H.-W. Kim, K.-Y. Cho, and M.-J. Youn, "An MRAS based diagnosis of open-circuit fault in PWM voltage-source inverters for PM synchronous motor drive systems," *IEEE Trans. Power Electron.*, vol. 28, no. 5, pp. 2514–2526, May 2013.

[7] B. Cai, Y. Zhao, H. Liu, and M. Xie, "A data-driven fault diagnosis methodology in three-phase inverters for PMSM drive systems," *IEEE Trans. Power Electron.*, vol. 32, no. 7, pp. 5590–5600, Jul. 2017.

[8] S. U. Jan, Y.-D. Lee, J. Shin, and I. Koo, "Sensor fault classification based on support vector machine and statistical time-domain features," *IEEE Access*, vol. 5, pp. 8682–8690, 2017.

[9] Z. Gao, C. Cecati, and S. X. Ding, "A survey of fault diagnosis and fault-tolerant techniques—Part I: Fault diagnosis with model-based and signal-based approaches," *IEEE Trans. Ind. Electron.*, vol. 62, no. 6, pp. 3757–3767, Jun. 2015.

[10] Z. Gao, C. Cecati and S. X. Ding, "A survey of fault diagnosis and fault-tolerant techniques—Part II: Fault diagnosis with knowledge-based and hybrid/active approaches," *IEEE Trans. Ind. Electron.*, vol. 62, no. 6, pp. 3768–3774, Jun. 2015.

[11] N. Wassinger, E. Penovi, R. G. Retegui, and S. Maestri, "Open-circuit fault identification method for interleaved converters based on time-domain analysis of the state observer residual," *IEEE Trans. Power Electron.*, vol. 34, no. 4, pp. 3740–3749, Apr. 2019.

[12] Y. Yu, Y. Zhao, B. Wang, X. Huang, and D. Xu, "Current sensor fault diagnosis and tolerant control for VSI-based induction motor drives," *IEEE Trans. Power Electron.*, vol. 33, no. 5, pp. 4238–4248, May 2018.

[13] H. Berriri, M. W. Naouar, and I. Slama-Belkhodja, "Easy and fast sensor fault detection and isolation algorithm for electrical drives," *IEEE Trans. Power Electron.*, vol. 27, no. 2, pp. 490–499, Feb. 2012.

[14] J. Poon, P. Jain, C. Spanos, S. K. Panda, and S. R. Sanders, "Fault prognosis for power electronics systems using adaptive parameter identification," *IEEE Trans. Ind. Appl.*, vol. 53, no. 3, pp. 2862–2870, May/Jun. 2017.

[15] S. Shao, P. W. Wheeler, J. C. Clare, and A. J. Watson, "Fault detection for modular multilevel converters based on sliding mode observer," *IEEE Trans. Power Electron.*, vol. 28, no. 11, pp. 4867–4872, Nov. 2013.

[16] D. U. Campos-Delgado and D. R. Espinoza-Trejo, "An observer-based diagnosis scheme for single and simultaneous open-switch faults in induction motor drives," *IEEE Trans. Ind. Electron.*, vol. 58, no. 2, pp. 671–679, Feb. 2011.

Authorized licensed use limited to: JACK YEH. Downloaded on June 20,2024 at 12:42:45 UTC from IEEE Xplore. Restrictions apply.

[17] B. Gou, X. Ge, S. Wang, X. Feng, J. B. Kuo, and T. G. Habetler, "An open-switch fault diagnosis method for single-phase PWM rectifier using a model-based approach in high-speed railway electrical traction drive system," *IEEE Trans. Power Electron.*, vol. 31, no. 5, pp. 3816–3826, May 2016.

[18] X. Ge, J. Pu, B. Gou, and Y.-C. Liu, "An open-circuit fault diagnosis approach for single-phase three-level neutral-point-clamped converters," *IEEE Trans. Power Electron.*, vol. 33, no. 3, pp. 2559–2570, Mar. 2018.

[19] A. B. Youssef, S. K. El Khil, and I. Slama-Belkhodja, "State observer-based sensor fault detection and isolation, and fault tolerant control of a single-phase PWM rectifier for electric railway traction," *IEEE Trans. Power Electron.*, vol. 28, no. 12, pp. 5842–5853, Dec. 2013.

[20] J. Xia, Y. Guo, B. Dai, and X. Zhang, "Sensor fault diagnosis and system reconfiguration approach for an electric traction PWM rectifier based on sliding mode observer," *IEEE Trans. Ind. Appl.*, vol. 53, no. 5, pp. 4768–4778, Sep./Oct. 2017.

[21] G. H. B. Foo, X. Zhang, and D. M. Vilathgamuwa, "A sensor fault detection and isolation method in interior permanent-magnet synchronous motor drives based on an extended Kalman filter," *IEEE Trans. Ind. Electron.*, vol. 60, no. 8, pp. 3485–3495, Aug. 2013.

[22] I. Hwang, S. Kim, Y. Kim, and C. E. Seah, "A survey of fault detection, isolation, and reconfiguration methods," *IEEE Trans. Control Syst. Technol.*, vol. 18, no. 3, pp. 636–653, May 2010.

[23] H. Zhao and L. Cheng, "Open-switch fault-diagnostic method for back-to-back converters of a doubly fed wind power generation system," *IEEE Trans. Power Electron.*, vol. 33, no. 4, pp. 3452–3461, Apr. 2018.

[24] B. Gou, X.-L. Ge, Y.-C. Liu, and X.-Y. Feng, "Load-current-based current sensor fault diagnosis and tolerant control scheme for traction inverters," *IET Electron. Lett.*, vol. 52, no. 20, pp. 1717–1719, Sep. 2016.

[25] D. Zhou, H. Qiu, S. Yang, and Y. Tang, "Submodule voltage similarity-based open-circuit fault diagnosis for modular multilevel converters," *IEEE Trans. Power Electron.*, vol. 34, no. 8, pp. 8008–8016, Aug. 2019.

[26] D. Zhou, S. Yang, and Y. Tang, "A voltage-based open-circuit fault detection and isolation approach for modular multilevel converters with model-predictive control," *IEEE Trans. Power Electron.*, vol. 33, no. 11, pp. 9866–9874, Nov. 2018.

[27] I. Abari, A. Lahouar, M. Hamouda, J. B. H. Slama, and K. Al-Haddad, "Fault detection methods for three-level NPC inverter based on dc-bus electromagnetic signatures," *IEEE Trans. Ind. Electron.*, vol. 65, no. 7, pp. 5224–5236, Jul. 2018.

[28] S. S. Moosavi, A. Djerdir, Y. Ait-Amirat, D. Arab Khaburi, and A. N'Diaye, "Artificial neural network-based fault diagnosis in the AC–DC converter of the power supply of series hybrid electric vehicle," *IET Elect. Syst. Transp.*, vol. 6, no. 2, pp. 96–106, Jun. 2016.

[29] T. Wang, H. Xu, J. G. Han, E. Elbouchikhi, and M. E. H. Benbouzid, "Cascaded H-bridge multilevel inverter system fault diagnosis using a PCA and multiclass relevance vector machine approach," *IEEE Trans. Power Electron.*, vol. 30, no. 12, pp. 7006–7018, Dec. 2015.

[30] S. Ye, J. Jiang, J. Li, Y. Liu, Z. Zhou, and C. Liu, "Fault diagnosis and tolerance control of five-level nested NPP converter using wavelet packet and LSTM," *IEEE Trans. Power Electron.*, vol. 35, no. 2, pp. 1907–1921, Feb. 2020.

[31] B. Gou, Y. Xu, Y. Xia, G. Wilson, and S. Liu, "An intelligent time-adaptive data-driven method for sensor fault diagnosis in induction motor drive system," *IEEE Trans. Ind. Electron.*, vol. 66, no. 12, pp. 9817–9827, Dec. 2019.

[32] I. Jlassi, J. O. Estima, S. K. El Khil, N. M. Bellaaj, and A. J. M. Cardoso, "A robust observer-based method for IGBTs and current sensors fault diagnosis in voltage-source inverters of PMSM drives," *IEEE Trans. Ind. Appl.*, vol. 53, no. 3, pp. 2894–2905, May/Jun. 2017.

[33] N. M. A. Freire, J. O. Estima, and A. J. M. Cardoso, "A new approach for current sensor fault diagnosis in PMSG drives for wind energy conversion systems," *IEEE Trans. Ind. Appl.*, vol. 50, no. 2, pp. 1206–1214, Mar./Apr. 2014.

[34] B. Lu and S. K. Sharma, "A literature review of IGBT fault diagnostic and protection methods for power inverters", *IEEE Trans. Ind. Appl.*, vol. 45, no. 5, pp. 1770–1777, Sep./Oct. 2009.

[35] M. Robnik-Sikonja and I. Kononenko, "Theoretical and empirical analysis of reliefF and RreliefF," *Mach. Learn.*, vol. 53, pp. 23–69, Oct. 2003.

[36] K. Kira and L.A. Rendell, "A practical approach to feature selection," in *Proc. 9th Int. Workshop Mach. Learn.*, 1992, pp. 249–256.

[37] Y.-H. Pao, G.-H. Park, and D. J. Sobajic, "Learning and generalization characteristics of the random vector functional-link net," *Neurocomputing*, vol. 6, no. 2, pp. 163–180, Apr. 1994.

Bin Gou (Member, IEEE) received the B.S. and Ph.D. degrees in electrical engineering from Southwest Jiaotong University, Chengdu, China, in 2010 and 2016, respectively.

He was a Visiting Student with the School of Electrical and Computer Engineering, Georgia Institute of Technology, Atlanta, GA, USA, from 2014 to 2015.

He was a Research Fellow with Rolls-Royce at NTU Corporate Laboratory, Nanyang Technological University, Singapore, from 2017 to 2020. He is currently with the School of Electrical Engineering, Southwest Jiaotong University, Chengdu, China. His research interests include data analytics for fault diagnosis and health management of power drive and energy storage systems.

Yan Xu (Senior Member, IEEE) received the B.E. and M.E degrees in electrical engineering from the South China University of Technology, Guangzhou, China, in 2008 and 2011, respectively, and the Ph.D. degree in electrical engineering from The University of Newcastle, Callaghan, NSW, Australia, in 2013.

He is currently the Nanyang Assistant Professor with the School of Electrical and Electronic Engineering, Nanyang Technological University (NTU), Singapore, and a Cluster Director at Energy Research Institute @ NTU, Singapore. Previously, he held The University of Sydney Postdoctoral Fellowship in Australia. His research interests include power system stability and control, microgrid, and data analytics for smart grid applications.

Dr. Xu is an Editor for the IEEE TRANSACTIONS ON SMART GRID, *CSEE Journal of Power and Energy Systems*, and an Associate Editor for *IET Generation, Transmission, and Distribution*.

Yang Xia (Student Member, IEEE) received the B.E. degree in electrical engineering from Xi'an Jiaotong University, Xi'an, China, in 2017, and the M.E. degrees from the Nanyang Technological University, Singapore, where is currently working toward the Ph.D. degree with the School of Electrical and Electronic Engineering.

His research interests include data analytics in fault detection and control of power systems.

Qingli Deng (Student Member, IEEE) received the B.S. degree in electrical engineering and automation from the Southwest Petroleum University, Chengdu, China, in 2018. She is currently working toward the M.S. degree in electrical engineering with the Southwest Jiaotong University, Chengdu, China.

Her research interests include fault diagnosis and fault tolerant of the traction converter systems.

Xinglai Ge (Member, IEEE) received the B.S., M.S., and Ph.D. degrees in electrical engineering from the Southwest Jiaotong University, Chengdu, China, in 2001, 2004, and 2010, respectively.

He is currently a Full Professor with the School of Electrical Engineering, Southwest Jiaotong University, and the Vice Director of the Department of Power Electronics and Power Drive. From July 2012 to August 2012, he was a Visiting Scholar with George Mason University, Fairfax, VA, USA. From 2013 to 2014, he was a Visiting Scholar with the School of Electrical and Computer Engineering, Georgia Institute of Technology, Atlanta, GA, USA. He has authored or coauthored more than 60 technical papers. His research interests include stability analysis and control of electrical traction systems, fault diagnosis, and hardware-in-the-loop simulation of traction converter and motor drive systems.

Authorized licensed use limited to: JACK YEH. Downloaded on June 20,2024 at 12:42:45 UTC from IEEE Xplore. Restrictions apply.